Available online at www.sciencedirect.com
ScienceDirect
Trans. Nonferrous Met. Soc. China 33(2023) 2761−2771
Transactions of Nonferrous Metals Society of China
www.tnmsc.cn

Facile synthesis of flower-like MoS_xSe_{2-x} nanocomposites for efficient hydrogen evolution

Hai-yan SHI[1], Yi WANG[2], De-zhi WANG[1]

1. School of Materials Science and Engineering, Central South University, Changsha 410083, China;
2. School of Materials Science and Engineering, Hunan University of Science and Technology, Xiangtan 411201, China

Received 30 November 2022; accepted 18 May 2023

Abstract: To solve the poor conductivity and limited active sites of $MoSe_2$, ternary MoS_xSe_{2-x} nanosheets with defects were synthesized by a convenient hydrothermal process. The results showed that the introduction of S element not only improved the electron transfer ability, but also provided more electrocatalytic active sites. Consequently, the optimized MoS_xSe_{2-x} with a S/Se molar ratio of 1:1 (MoSSe) presented superior electrocatalytic hydrogen evolution reaction performance with a low Tafel slope of 47 mV/dec, and a small overpotential of −165 mV at −10 mA/cm^2 as well as good durability. This work provides an additional route for better understanding the modulation of multi-factors in designing and synthesizing $MoSe_2$-based catalysts to improve their electrochemical activity.

Key words: ternary MoS_xSe_{2-x} alloy; defect; synergistic effect; electrocatalyst; hydrogen evolution

1 Introduction

With the deterioration of the global environment, climate warming and increasing energy crisis, it is urgent to seek a clean energy to replace the current fossil fuels. Hydrogen, a renewable clean energy, is considered as a promising alternative to traditional energy [1−5]. Electrochemical water splitting is a simple, effective and environmentally friendly method for hydrogen production [6,7]. In order to maximize the efficiency of hydrogen production and the application of hydrogen energy, highly efficient and low-cost electrocatalysts are indispensable [8−12].

Two-dimensional (2D) transition metal dichalcogenides (TMDCs), which are low-cost, robust and earth-abundant electrocatalysts, have been investigated extensively as the candidates of electrocatalysts for hydrogen evolution reaction (HER) [9,13]. Amongst, $MoSe_2$, similar to MoS_2, is attracting more and more attention as a promising and efficient HER catalyst due to its tunable structure and properties [14]. Nevertheless, poor electrical conductivity and limited active sites of bulk $MoSe_2$ greatly restrict its electrochemical performance. Various strategies or techniques have been explored to further enhance its electrocatalytic activity, such as crystal structure modulation [15,16], defect engineering [17,18], morphology regulation [19,20], interface construction [21,22], heteroatom doping [23,24], and alloying [25], or integration with conductive medium [15,26]. Previous studies indicated that alloying by introducing another element to form ternary compounds is an effective strategy to enhance electrocatalytic HER performance of $MoSe_2$ [27,28]. In addition, adjusting the free energy change of hydrogen adsorption (ΔG_{H^*}) is also extremely important for optimizing the hydrogen evolution performance of electrocatalysts [29]. The ΔG_{H^*} on selenized Mo edges, which is equal to −140 meV, is

Corresponding author: Yi WANG, Tel: +86-731-58290888, E-mail: ywang312@hnust.edu.cn;
De-zhi WANG, Tel: +86-731-88830202, E-mail: dzwang@csu.edu.cn
DOI: 10.1016/S1003-6326(23)66296-X

slightly strong, whereas that on sulfided Mo edges is slightly weak (ΔG_{H^*}=80 meV) [30,31]. Thus, it would be possible to attain a thermoneutral state ($\Delta G_{H^*} \approx 0$) by reasonably designing and developing MoS_xSe_{2-x} ternary alloys with changing S/Se molar ratios. Several pioneering studies on ternary MoS_xSe_{2-x} alloys, which were synthesized by different techniques including chemical vapor deposition (CVD) [32], hot injection [33], and hydrothermal or solvothermal synthesis [34,35], have been reported. Although the HER performance of $MoSe_2$ can be improved to a certain extent by introducing S element, there is still much room to promote the overall electrocatalytic HER performance. Consequently, it is still great challenging to explore a simple and feasible technique to synthesize $MoSe_2$-based HER electrocatalysts with enhanced conductivity and improved electrocatalytic activity of active sites to synergistically boost their HER properties.

Recently, a nanoflower-structured 1T/2H $MoSe_2$ has been synthesized by a convenient hydrothermal process, which has achieved the synergistic regulation of conductivity and active sites, and improved the electrocatalytic HER [36]. Here, unique ternary MoS_xSe_{2-x} nanosheets with rich defects were prepared by a modified hydrothermal method. The excellent electrocatalytic HER performance was obtained by adjusting the ratio of S and Se elements. The synergistic modulation acquired by a simple and effective method in this work provides a facile route to improve the electrochemical activity of $MoSe_2$.

2 Experimental

2.1 Preparation of MoS_xSe_{2-x}

A certain amount of Se powder was dissolved in 8 mL of hydrazine hydrate, marked it as Solution A. 1 mmol of $Na_2MoO_4·2H_2O$ and a certain amount of thioacetamide were completely dissolved in 42 mL of distilled water, marked it as Solution B. After that, Solution A was slowly added to Solution B, and then the mixture was poured into a 100 mL hydrothermal reactor, which was subsequently put into an oven at 220 °C for 12 h. The products in the autoclave were naturally cooled to room temperature, and then the samples were collected with vacuum filtration, washed with anhydrous ethanol and distilled water, dried at 60 °C for 12 h. The total amount of Se powder and thioacetamide was 2 mmol. According to the amount of thioacetamide (0.4, 1, and 1.6 mmol), the obtained samples were named $MoS_{0.4}Se_{1.6}$, MoSSe, and $MoS_{1.6}Se_{0.4}$, respectively.

2.2 Structural characterization

X-ray diffraction (XRD) measurements (Rigaku D/Max−2500) were performed to obtain information about the composition and structure of the products. The surface information of the products was collected by X-ray photoelectron spectroscopy (XPS, ESCALAB 250Xi). The morphology and microstructure of the as-obtained products were observed by transmission electron microscopy (TEM, FEI Tecnai G2 F20).

2.3 Electrochemical measurements

The electrocatalytic HER performance of the as-obtained products was surveyed using a standard three-electrode cell, where a 3 mm glassy carbon electrode coated with the products, saturated calomel electrode and graphite rod, was used as working, reference and counter electrodes, respectively. Typically, the products were ultrasonically dispersed in a mixed ethanol−water solution (1:4, volume ratio) containing a Nafion solution (5 wt.%) to obtain a uniform ink. A droplet of the homogeneous ink (5 μL, 2.78 mg/mL) was deposited onto a working electrode. The product loading was about 0.21 mg/cm^2. Commercially obtained 20 wt.% Pt/C was used as a reference catalyst. All measurements were performed in a 0.5 mol/L H_2SO_4 solution. The electrochemical double-layer capacitance (C_{dl}) was assessed by the cyclic voltammetry (CV). Linear sweep voltammetry (LSV) was implemented at 2 mV/s. Electrochemical impedance spectroscopy (EIS) was performed from 1000 kHz to 1 Hz at 200 mV. The electrochemical stability was evaluated by cycling the electrodes 1000 times, and chronoamperometric curve was also measured at a current density of −10 mA/cm^2.

3 Results and discussion

3.1 Material characterization

The morphological feature of MoSSe was observed by TEM. MoSSe presents a typical flower-like morphology assembled by interconnected

curved nanosheets (Figs. 1(a, b)). These curved nanosheets on the surface provide abundant edge sites for improving the performance of electrochemical catalyst.

The microstructure of the catalyst was further characterized by high-resolution transmission electron microscopy (HRTEM), and the twisted nanosheets have a typical few-layer structure (Figs. 1(c, d)). The interlayer spacing between adjacent layers is approximately 0.67 nm, which is close to that of 2H-phase $MoSe_2$ (002) crystal plane (0.65 nm) (Fig. 1(c)) [15]. The lattice fringes of the (002) crystal plane are discontinuous, indicating that defects are dispersed in the product [37,38], as shown in Figs. 1(c) and (d). Therefore, a large number of nano-regions appear along the basal planes. In addition, an average interplanar spacing of 0.28 nm is found in Fig. 1(d), corresponding to the (100) plane in 2H-phase $MoSe_2$ [39]. Moreover, the directions of the (100) crystal plane on the basal plane are not consistent, disclosing that a relatively disordered atomic arrangement exists on the basal plane. The disordered arrangement of atoms leads to cracks in the basal planes, thereby generating additional edge sites [40,41]. Furthermore, discontinuous and twisted lattice fringes were also observed, showing the existence of defect structure [42,43]. Such a defect structure provides more catalytic sites, improving the electrocatalytic HER performance.

The XRD patterns of samples are shown in Fig. 2. The two diffraction peaks of $MoSe_2$ correspond to the (100) and (110) crystal planes, respectively. And the diffraction peak corresponding to (002) crystal plane is not observed. Compared with the standard XRD pattern of 2H-phase $MoSe_2$ (JCPDS No. 29-0914), the diffraction peak of the (100) crystal plane shifts to the right, which is consistent with the results reported previously, indicating the presence of 1T-phase $MoSe_2$ in the sample [44]. The diffraction peaks corresponding to (002), (100) and (110)

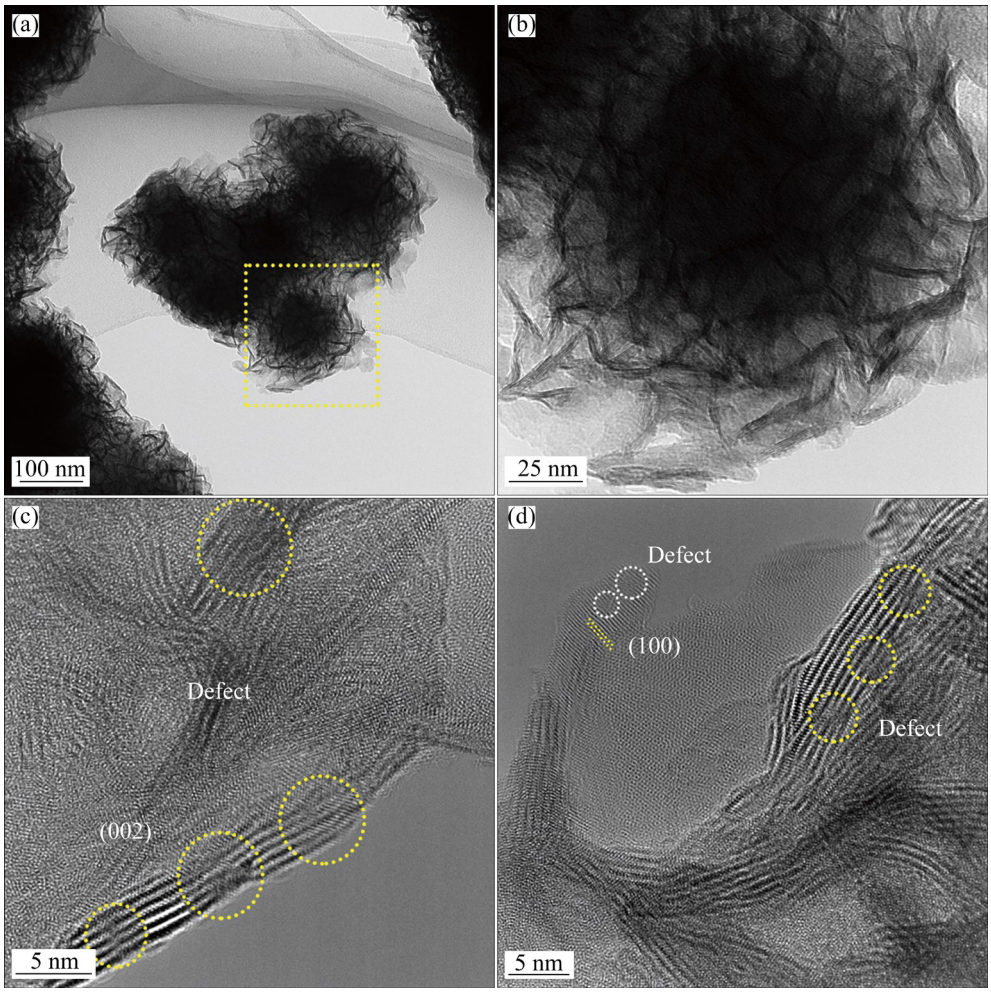

Fig. 1 Microstructures of MoSSe: (a, b) TEM images; (c, d) HRTEM images

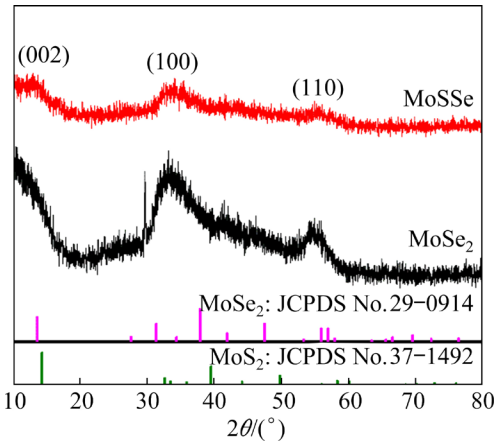

Fig. 2 XRD patterns of samples

crystal planes were detected in the XRD pattern of MoSSe sample. Compared with $MoSe_2$, it is found that the diffraction peaks of MoSSe sample shift to a higher angle as a whole, which may be caused by the smaller radius of S^{2-}-introduced sample than that of Se^{2-}-introduced sample [33,34].

To further study the elemental composition and valence state of elements on the surfaces of $MoSe_2$ and MoSSe, the XPS analysis was carried out. The full spectra reveal the presence of Mo and Se elements in $MoSe_2$, and the presence of Mo, Se and S elements in MoSSe (Fig. 3(a)). The high resolution XPS spectra of Mo 3d are shown in Fig. 3(b). After deconvoluting the Mo 3d spectrum, two pairs of double peaks at 228.3, 231.4, 229.0 and 232.1 eV can be attributed to the 1T-phase and 2H-phase of $MoSe_2$ [36,45], respectively, while the small double peaks at 229.9 and 233.0 eV can be assigned to the amorphous phase $MoSe_3$ [44,46]. The double peaks (232.9 and 236.0 eV) at high binding energy should be ascribed to Mo^{6+} [46], which is caused by the surface oxidation as the sample is exposed to air. In addition, the smaller single peak at 230.0 eV corresponds to the binding energy of Se 3s [44], and the other smaller single peak at 226.9 eV belongs to S 2s of S^{2-} [47].

The Se 3d spectrum of $MoSe_2$ (Fig. 3(c)) exhibits two pairs of double peaks at 54.3, 55.2, 55.0 and 55.9 eV, corresponding to 1T-phase and 2H-phase of $MoSe_2$ [48], respectively. And only one pairs of double peaks at 54.5 and 55.4 eV can be

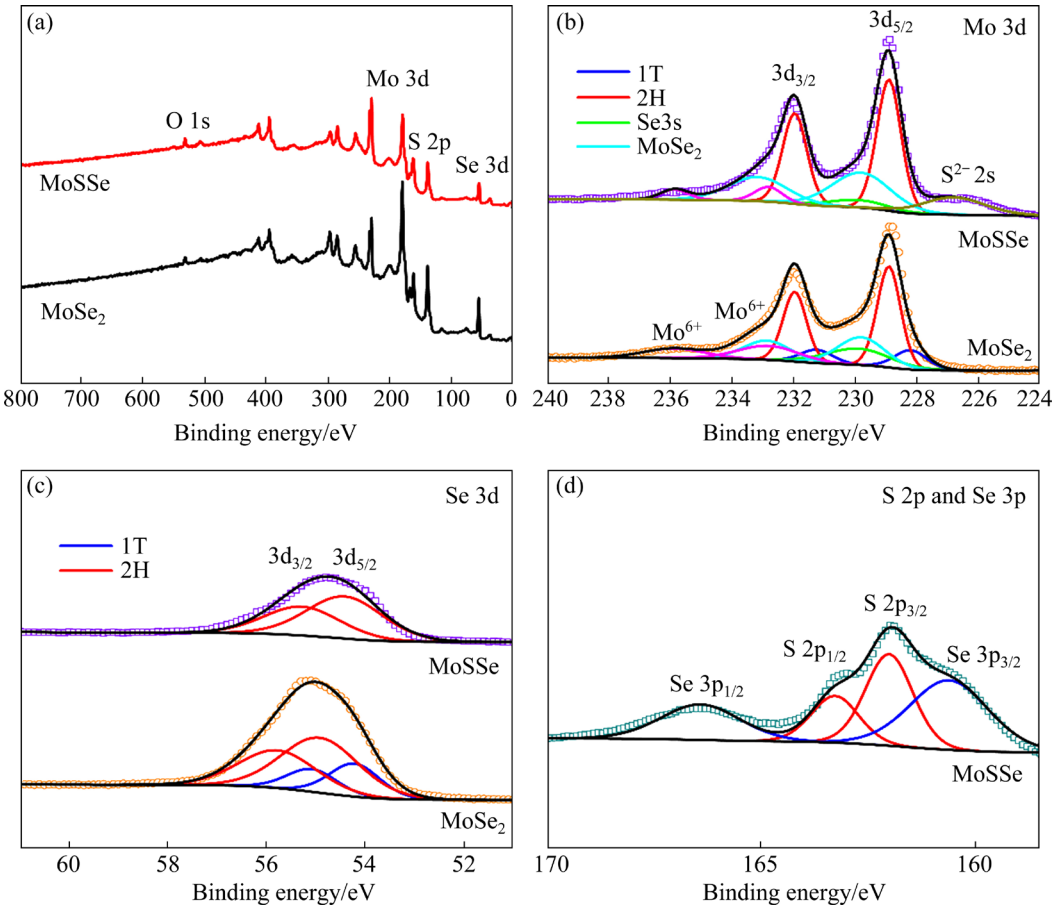

Fig. 3 XPS spectra of MoSSe and $MoSe_2$: (a) Survey pattern; (b) Mo 3d; (c) Se 3d; (d) S 2p and Se 3p

found in MoSSe. Two pairs of double peaks can be observed after deconvoluting the XPS spectrum of S 2p (Fig. 3(d)). The double peaks at 161.1 and 166.9 eV correspond to Se $2p_{3/2}$ and Se $2p_{1/2}$ of Se^{2-}, while the other two peaks at 162.1 and 163.4 eV are indexed to the binding energies of S $2p_{3/2}$ and S $2p_{1/2}$ of S^{2-}, respectively [38]. The result indicates that Mo—S bond is formed in the sample.

3.2 Electrochemical performances

The HER electrochemical performance of as-obtained samples was investigated. Figure 4(a) shows the polarization curves of the samples. Compared with $MoSe_2$ and MoS_2, MoSSe catalyst displays the best hydrogen evolution performance. As can be seen from Table 1, MoSSe achieves a current density of −10 mA/cm^2 at an overpotential of −165 mV, which has increments of 44 and 57 mV in comparison to $MoSe_2$ (−209 mV) and MoS_2 (−222 mV), respectively.

The Tafel slope derived from the LSV curve can reflect chemical reactivity in the HER. Commonly, three different Tafel slopes (118, 39 and 29 mV/dec) correspond to the rate-determining step in HER following the Volmer reaction, Heyrovsky reaction and Tafel reaction, respectively. MoSSe exhibits a smaller Tafel slope of 47 mV/dec (Fig. 4(b)) than $MoSe_2$ (65 mV/dec) and MoS_2 (64 mV/dec), indicating a faster hydrogen generation rate of MoSSe catalyst. According to the value of Tafel slope, MoSSe follows a Volmer–Heyrovsky reaction mechanism, and the electrochemical desorption is the HER rate-controlling step. The HER performance of MoSSe and reported similar materials have been summarized in Table 1.

In order to better understand the difference of the hydrogen evolution performance among the samples, the effective electrochemical active surface area (ECSA), which is represented using the

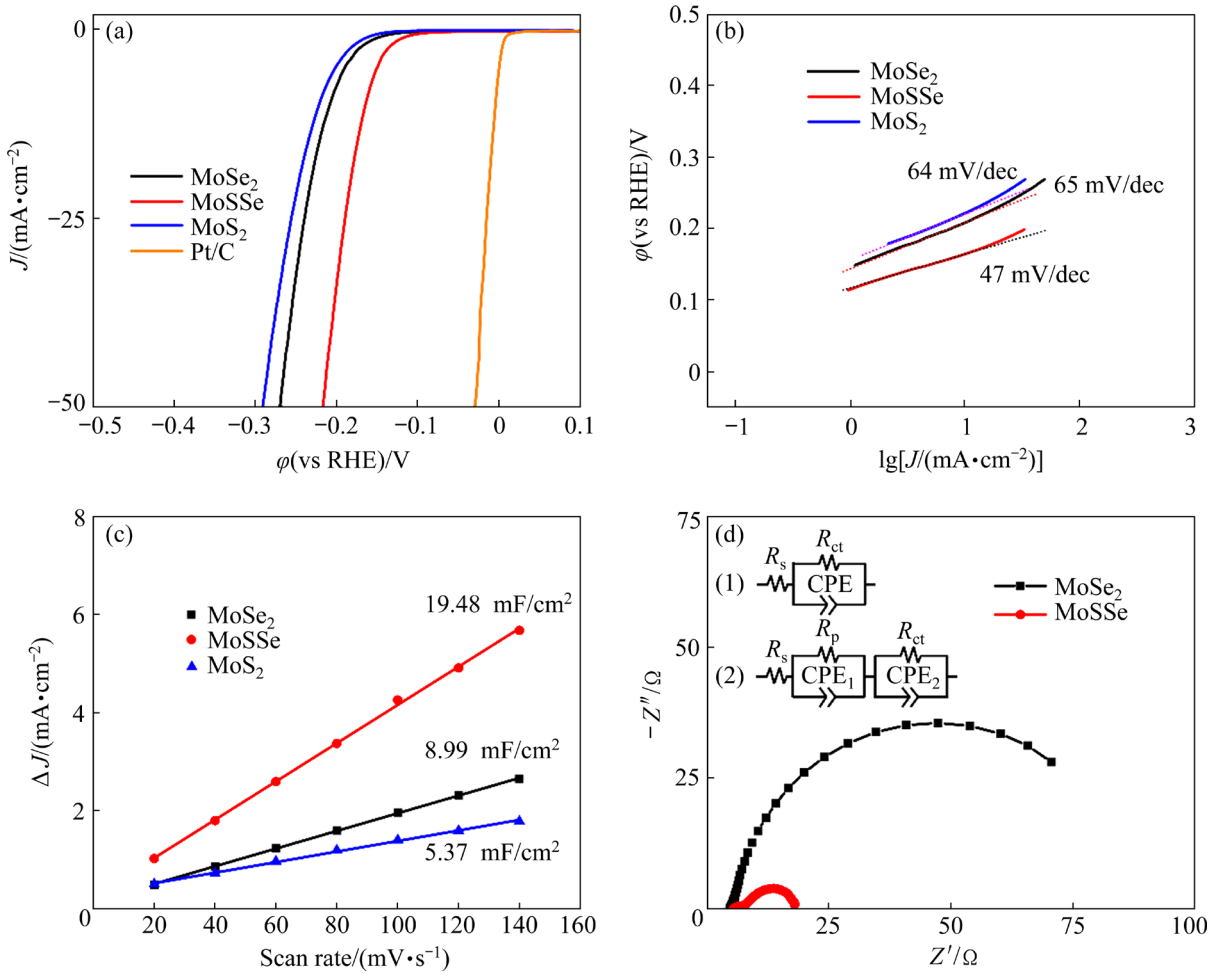

Fig. 4 Electrochemical performances of $MoSe_2$, MoSSe and MoS_2 synthesized under same conditions: (a) Polarization curves; (b) corresponding Tafel plots of samples stemming from (a); (c) Capacitive current density (ΔJ) at different scan rates; (d) Nyquist plots of samples

Table 1 Electrochemical HER performance comparison of different catalysts

Catalyst	Overpotential at −10 mA/cm^2/mV	Tafel slope/(mV·dec^{-1})	Ref.
MoSSe	−165	47	This work
MoSSe/rGO	−285	98	[49]
$MoSe_2$−Ni_3Se_4	−203	57	[50]
$MoSe_2$	−300	90	[18]
$MoSe_2$-ts@MoS_2-ts	−186	71	[51]
B−1T $MoSe_2$	−180	50.6	[23]
Ni−$MoSe_2$	−226	94.5	[52]
Co−$MoSe_2$	−210	90.9	[52]
$MoSe_2$/MoS_2	−162	61	[53]
$MoSe_2$@MoS_2	−161	60	[54]

value of C_{dl} due to the linearly proportional relation of their values, was investigated. C_{dl} is derived by testing the cyclic voltammetry curves of the sample (Fig. 5).

The relationship between capacitive current density and scan rate is presented in Fig. 4(c). MoSSe also presents a higher value of C_{dl} (19.48 mF/cm^2) in comparison to $MoSe_2$ (8.99 mF/cm^2) and MoS_2 (5.37 mF/cm^2), indicating that the structure of nanosheets with defects affords more exposed surface active sites and enhances the electrocatalytic HER activity [55].

The hydrogen evolution kinetics of the samples was further studied by electrochemical impedance spectroscopy (Fig. 4(d)). The charge transfer resistance (R_{ct}) is obtained by fitting the Nyquist plots with a suitable circuit model. The R_{ct} value of MoSSe is 10.9 Ω, which is approximately 12.8% that of $MoSe_2$ (85.1 Ω), indicating a faster electron transfer rate for MoSSe sample, which is conducive to the hydrogen evolution reaction kinetics. Thus, the conductivity and exposed active sites of the electrocatalyst can be improved by alloying [56,57].

The long-term stability of MoSSe catalyst was tested by cyclic CV scanning and chrono-potentiometry testing. Figure 6 shows that the current density change could be ignored after 1000 CV cycles, and the time-dependent current curve was maintained at a current density of −10 mA/cm^2 for at least 6 h (the inset in Fig. 6), suggesting an outstanding stability of MoSSe.

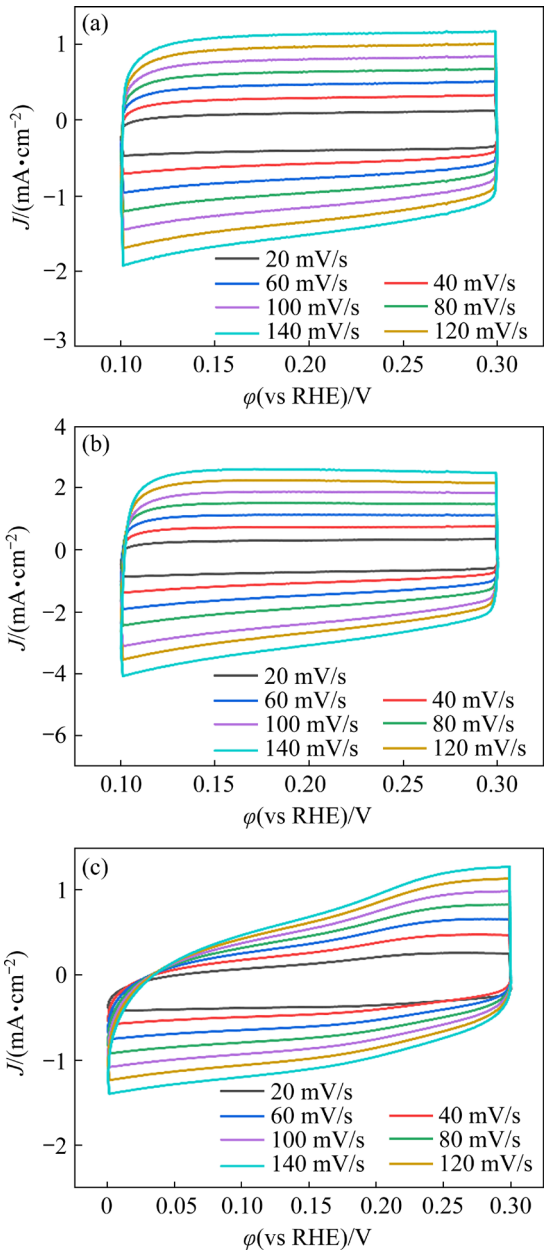

Fig. 5 CV curves at varied scan rates: (a) $MoSe_2$; (b) MoSSe; (c) MoS_2

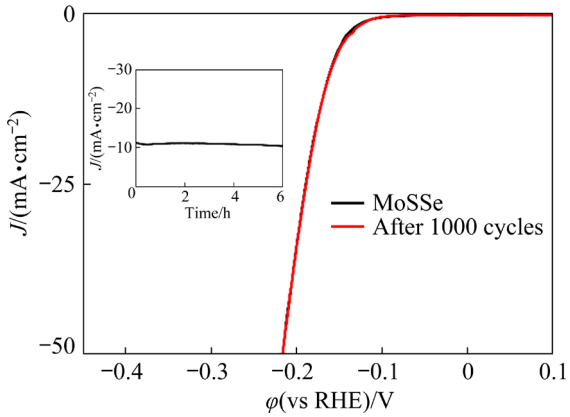

Fig. 6 Electrochemical stability test results of as-prepared MoSSe

Furthermore, the effect of S/Se molar ratio on the electrochemical HER properties was also investigated. Figure 7(a) shows the polarization curves of the obtained samples. Compared with $MoS_{0.4}Se_{1.6}$ and $MoS_{1.6}Se_{0.4}$, MoSSe also shows the best hydrogen evolution performance with the lowest initial overpotential (−116 mV) and the lowest overpotential to achieve the current density of −10 mA/cm^2.

Figure 7(b) shows that the Tafel slopes of $MoS_{0.4}Se_{1.6}$ (50 mV/dec) and $MoS_{1.6}Se_{0.4}$ (60 mV/dec) are higher than that of MoSSe, demonstrating that MoSSe possesses faster hydrogen evolution reaction rate and better hydrogen evolution performance.

To further understand the effect of S/Se molar ratio on the electrochemical HER properties of as-obtained samples, the ECSA values of the samples were estimated by surveying C_{dl}, which is derived by testing the cyclic voltammetry curves of the sample (Fig. 8). In comparison with $MoS_{0.4}Se_{1.6}$ (8.76 mF/cm^2) and $MoS_{1.6}Se_{0.4}$ (16.78 mF/cm^2), MoSSe also displays the highest the C_{dl} value (19.48 mF/cm^2), revealing that MoSSe has more active sites and better catalytic performance.

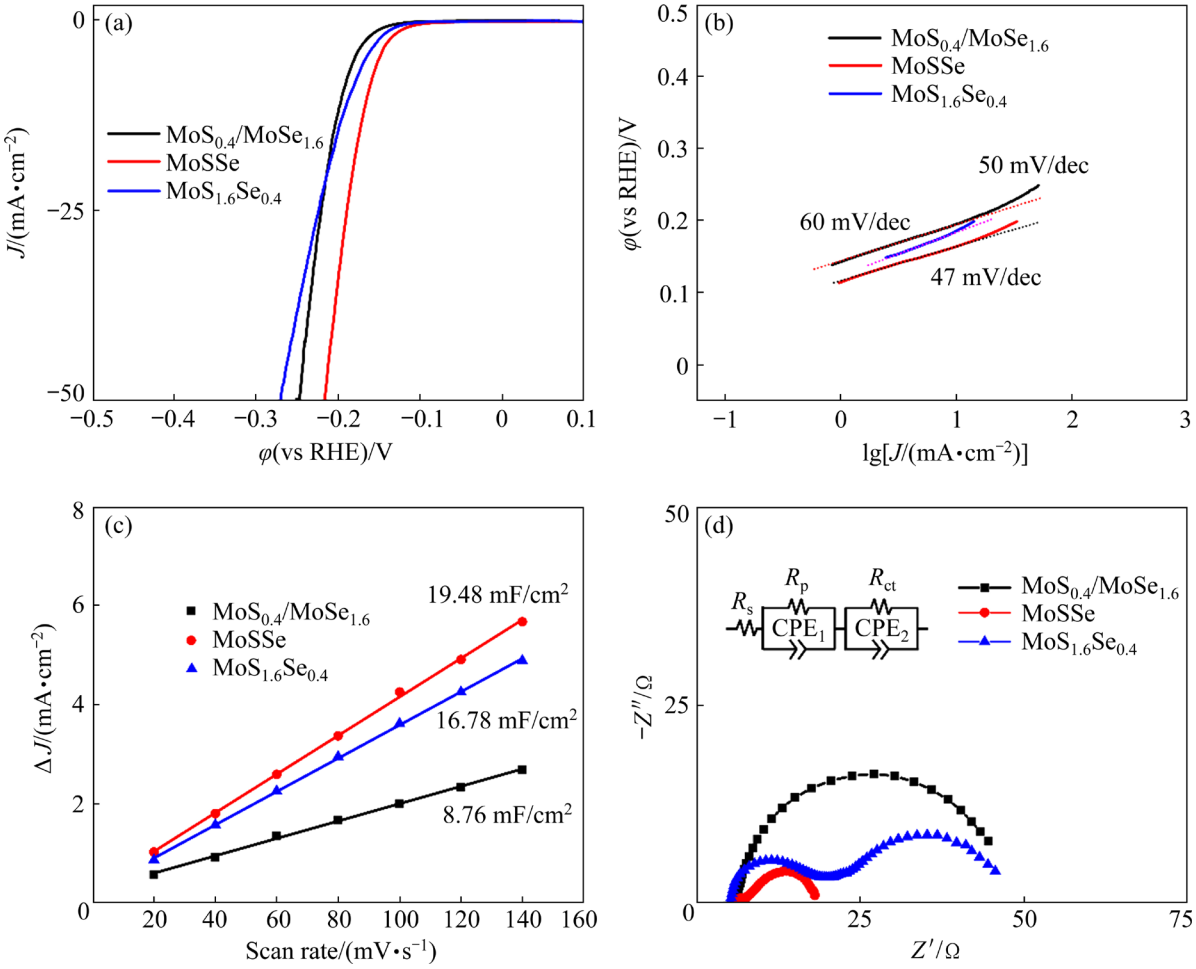

Fig. 7 Electrochemical performances of MoS_xSe_{2-x} synthesized at varied molar ratios of S to Se: (a) Polarization curves; (b) Corresponding Tafel plots of samples stemming from (a); (c) Capacitive current density at different scan rates; (d) Nyquist plots of samples

Table 2 Electrochemical HER performance comparison of different samples

Sample	Overpotential at −10 mA/cm^2/mV	Tafel slope/(mV·dec^{-1})	Initial overpotential at −1 mA/cm^2/mV
$MoS_{0.4}Se_{1.6}$	−196	50	−144
MoSSe	−165	47	−116
$MoS_{1.6}Se_{0.4}$	−188	60	−130

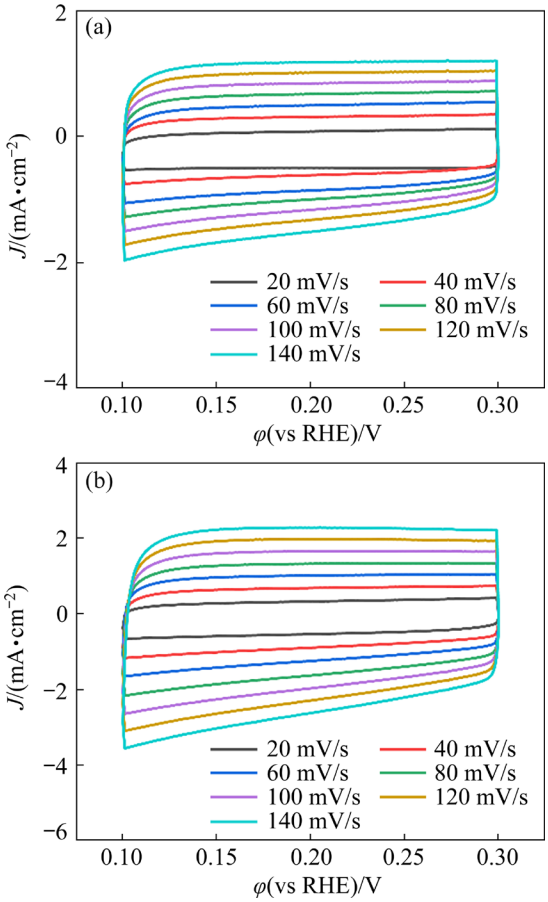

Fig. 8 CV curves of $MoS_{0.4}Se_{1.6}$ (a) and $MoS_{1.6}Se_{0.4}$ (b)

The kinetics of hydrogen evolution reaction was further studied by electrochemical impedance spectroscopy (Fig. 7(d)). The R_{ct} values of $MoS_{0.4}Se_{1.6}$, MoSSe and $MoS_{1.6}Se_{0.4}$ are 40.7, 10.9 and 36.4 Ω, respectively, indicating that MoSSe possesses the fastest HER process. The results reveal that intrinsic conductivity and exposed catalytically active sites can be enhanced by tuning the component ratio, and their synergistic effect leads to improving the electrocatalytic HER performance.

4 Conclusions

(1) The ternary MoS_xSe_{2-x} nanosheets with defects were synthesized by a convenient hydrothermal process and served as electrocatalysts for HER.

(2) The electron transfer ability and active sites of the MoS_xSe_{2-x} electrocatalysts were increased simultaneously at right S/Se molar ratio.

(3) The MoS_xSe_{2-x} with a S/Se molar ratio of 1:1 exhibits the best HER activity, a low overpotential (−165 mV) at −10 mA/cm^2 and a small Tafel slope (47 mV/dec).

Acknowledgments

This work was supported by the Natural Science Foundation of Hunan Province, China (No. 2020JJ4730).

References

[1] YUE Mei-ling, LAMBERT H, PAHON E, ROCHE R, JEMEI S, HISSEL D. Hydrogen energy systems: A critical review of technologies, applications, trends and challenges [J]. Renewable and Sustainable Energy Reviews, 2021, 146: 111180.

[2] YU Zi-you, DUAN Yu, FENG Xing-yu, YU Xing-xing, GAO Min-rui, YU Shu-hong. Clean and affordable hydrogen fuel from alkaline water splitting: Past, recent progress, and future prospects [J]. Advanced Materials, 2021, 33: e2007100.

[3] LI Shuo, XIONG Jin-yan, ZHU Xue-teng, LI Wei-jie, CHEN Rong, CHENG Gang. Recent advances in synthesis strategies and solar-to-hydrogen evolution of 1T phase MS_2 (M=W, Mo) co-catalysts [J]. Journal of Materials Science & Technology, 2022, 101: 242−263.

[4] ZENG Jian, XU Liang, LUO Xin, CHEN Tong, TANG Shuai-hao, HUANG Xin, WANG Ling-ling. Z-scheme systems of ASi_2N_4 (A = Mo or W) for photocatalytic water splitting and nanogenerators [J]. Tungsten, 2022, 4(1): 52−59.

[5] HUO Wen-yi, WANG Shi-qi, ZHU Wen-han, ZHANG Ze-ling, FANG Feng, XIE Zong-han, JIANG Jian-qing. Recent progress on high-entropy materials for electrocatalytic water splitting applications [J]. Tungsten, 2021, 3(2): 161−180.

[6] LI Lei-gang, WANG Peng-tang, SHAO Qi, HUANG Xiao-qing. Metallic nanostructures with low dimensionality for electrochemical water splitting [J]. Chemical Society Reviews, 2020, 49: 3072−3106.

[7] CHEN Ya-qiong, ZHANG Jin-feng, WAN Lei, HU Wen-bin, LIU Lei, ZHONG Cheng, DENG Yi-da. Effect of nickel phosphide nanoparticles crystallization on hydrogen evolution reaction catalytic performance [J]. Transactions of Nonferrous Metals Society of China, 2017, 27: 369−376.

[8] XU Yuan-lin, WANG Chen, HUANG Yun-hui, FU Jing. Recent advances in electrocatalysts for neutral and large-current-density water electrolysis [J]. Nano Energy, 2021, 80: 105545.

[9] FU Qiang, HAN Jie-cai, WANG Xian-jie, XU Ping, YAO Tai, ZHONG Jun, ZHONG Wen-wu, LIU Sheng-wei, GAO Tang-ling, ZHANG Zhi-hua, XU Ling-ling, SONG Bo. 2D transition metal dichalcogenides: Design, modulation, and challenges in electrocatalysis [J]. Advanced Materials, 2021, 33: 1907818.

[10] WANG Fei-hong, DONG Bin-bin, WANG Jun-wei, KE Nian-wang, TAN Chun-tian, HUANG An-ding, WU Yu-tong, HAO Lu-yuan, YIN Liang-jun, XU Xin, XIAN Yu-xi, AGATHOPOULOS S. Self-supported porous heterostructure

WC/WO_{3-x} ceramic electrode for hydrogen evolution reaction in acidic and alkaline media [J]. Journal of Advanced Ceramics, 2022, 11: 1208−1221.

[11] TANG Jian, XU Ji-lin, LI Liang-liang, MA Yong-cun, YE Zhi-guo, LUO Hong-yu, LUO Jun-ming. In-situ hydrothermal synthesis of Ni−MoO_2 heterostructure on porous bulk NiMo alloy for efficient hydrogen evolution reaction [J]. Transactions of Nonferrous Metals Society of China, 2022, 32: 1598−1608.

[12] REN Yu-xi, ZHU Sheng-li, LIANG Yan-qin, LI Zhao-yang, WU Shui-lin, CHANG Chun-tao, LUO Shui-yuan, CUI Zhen-duo. Hierarchical Ni_3S_4@MoS_2 nanocomposites as efficient electrocatalysts for hydrogen evolution reaction [J]. Journal of Materials Science & Technology, 2021, 95: 70−77.

[13] LIN Liang-xu, SHERRELL P, LIU Yu-qing, LEI Wen, ZHANG Shao-wei, ZHANG Hai-jun, WALLACE G G, CHEN Jun. Engineered 2D transition metal dichalcogenides—A vision of viable hydrogen evolution reaction catalysis [J]. Advanced Energy Materials, 2020, 10: 1903870.

[14] KWON I S, KWAK I H, DEBELA T T, ABBAS H G, PARK Y C, AHN J P, PARK J, KANG H S. Se-rich $MoSe_2$ nanosheets and their superior electrocatalytic performance for hydrogen evolution reaction [J]. ACS Nano, 2020, 14: 6295−6304.

[15] YANG Chun-ming, ZHOU Li-hai, WANG Chuan-tao, DUAN Wen, ZHANG Le, ZHANG Fu-chun, ZHANG Jun-jun, ZHEN Yan-zhong, GAO Lou-jun, FU Feng, LIANG Yu-cang. Large-scale synthetic Mo@(2H-1T)−$MoSe_2$ monolithic electrode for efficient hydrogen evolution in all pH scale ranges and seawater [J]. Applied Catalysis B: Environmental, 2022, 304: 120993.

[16] XUE Yan-qin, XU Yan-yan, YAN Qing, ZHU Kai, YE Ke, YAN Jun, WANG Qian, CAO Dian-xue, WANG Gui-ling. Coupling of Ru nanoclusters decorated mixed-phase (1T and 2H) $MoSe_2$ on biomass-derived carbon substrate for advanced hydrogen evolution reaction [J]. Journal of Colloid and Interface Science, 2022, 617: 594−603.

[17] XIAO De-zhi, BAO De-liang, LIANG Xiong-yi, WANG Ying, SHEN Jie, CHENG Cheng, CHU P K. Experimental and theoretical investigation of the control and balance of active sites on oxygen plasma-functionalized $MoSe_2$ nanosheets for efficient hydrogen evolution reaction [J]. Applied Catalysis B: Environmental, 2021, 288: 119983.

[18] TRUONG Q D, NAKAYASU Y, NGUYEN Q T, NGUYEN D N, NGUYEN C T, DEVARAJU M K, RANGAPPA D, NAYUKI K, SASAKI Y, TRAN P D, TOMAI T, HONMA I. Defect-rich exfoliated $MoSe_2$ nanosheets by supercritical fluid process as an attractive catalyst for hydrogen evolution in water [J]. Applied Surface Science, 2020, 505: 144537.

[19] LI Chang-dian, ZHU Li-li, LI Han, LI Hui, WU Zi-qiang, LIANG Chang-hao, ZHU Xue-bin, SUN Yu-ping. Dual surfactants applied in synthesis of $MoSe_2$ for high-efficiency hydrogen evolution reaction [J]. Journal of Alloys and Compounds, 2021, 863: 158092.

[20] VATTIKUTI S V P, DEVARAYAPALLI K C, NAGAJYOTHI P C, SHIM J. Microwave synthesized dry leaf-like mesoporous $MoSe_2$ nanostructure as an efficient catalyst for enhanced hydrogen evolution and supercapacitor applications [J]. Microchemical Journal, 2020, 153: 104446.

[21] ZHANG Li-li, LEI Yuan-ting, ZHOU Dan-ni, XIONG Cheng-li, JIANG Zhuo-li, LI Xin-yuan, SHANG Hui-shan, ZHAO Ya-fei, CHEN Wen-xing, ZHANG Bing. Interfacial engineering of 3D hollow $CoSe_2$@ultrathin $MoSe_2$ core@shell heterostructure for efficient pH-universal hydrogen evolution reaction [J]. Nano Research, 2022, 15: 2895−2904.

[22] PATEL A B, VAGHASIYA J V, CHAUHAN P, SUMESH C K, PATEL V, SONI S S, PATEL K D, GARG P, SOLANKI G K, PATHAK V M. Synergistic 2D $MoSe_2$@WSe_2 nanohybrid heterostructure toward superior hydrogen evolution and flexible supercapacitor [J]. Nanoscale, 2022, 14: 6636−6647.

[23] MAO Ze-yang, WANG Chao, LU Hao-liang, TANG Kai, LI Qun, YAN Cheng-lin, WANG Xian-fu. Boron-modified electron transfer in metallic 1T $MoSe_2$ for enhanced inherent activity on per-catalytic site toward hydrogen evolution [J]. Advanced Materials Interfaces, 2020, 7: 1901560.

[24] YANG Ya-qian, ZHAO Xu, MAO Han, NING Rui, ZHENG Xiao-hang, SUI Jie-he, CAI Wei. Nickel-doped $MoSe_2$ nanosheets with Ni−Se bond for alkaline electrocatalytic hydrogen evolution [J]. International Journal of Hydrogen Energy, 2020, 45: 10724−10728.

[25] KWON I S, KWAK I H, KIM J Y, DEBELA T T, PARK Y C, PARK J, KANG H S. Concurrent vacancy and adatom defects of $Mo_{1-x}Nb_xSe_2$ alloy nanosheets enhance electrochemical performance of hydrogen evolution reaction [J]. ACS Nano, 2021, 15: 5467−5477.

[26] POORAHONG S, SOMNIN C, MALAM M I, DUBOIS C, CHERGUI S, PENG Zhi-yuan, SU Yi-lu, XUAN T T, THAMMAKHET-BURANACHAI C, MAZZAH A, SIAJ M. Nanoporous graphite-like membranes decorated with $MoSe_2$ nanosheets for hydrogen evolution [J]. ACS Applied Nano Materials, 2022, 5: 2769−2778.

[27] VIKRAMAN D, HUSSAIN S, RABANI I, FEROZE A, ALI M, SEO Y S, CHUN S H, JUNG J, KIM H S. Engineering $MoTe_2$ and Janus SeMoTe nanosheet structures: First-principles roadmap and practical uses in hydrogen evolution reactions and symmetric supercapacitors [J]. Nano Energy, 2021, 87: 106161.

[28] BAR-ZIV R, MEIRON O E, BAR-SADAN M. Enhancing the catalytic activity of the alkaline hydrogen evolution reaction by tuning the S/Se ratio in the $Mo(S_xSe_{1-x})_2$ catalyst [J]. Nanoscale, 2018, 10: 16211−16216.

[29] MEIRON O E, KURAGANTI V, HOD I, BAR-ZIV R, BAR-SADAN M. Improved catalytic activity of $Mo_{1-x}W_xSe_2$ alloy nanoflowers promotes efficient hydrogen evolution reaction in both acidic and alkaline aqueous solutions [J]. Nanoscale, 2017, 9: 13998−14005.

[30] TANG Hao, DOU Kun-peng, KAUN Chao-Cheng, KUANG Qing, YANG Shi-he. $MoSe_2$ nanosheets and their graphene hybrids: Synthesis, characterization and hydrogen evolution reaction studies [J]. Journal of Materials Chemistry A, 2014, 2: 360−364.

[31] JARAMILLO T F, JØRGENSEN K P, BONDE J, NIELSEN J H, HORCH S, CHORKENDORFF I. Identification of active edge sites for electrochemical H_2 evolution from MoS_2 nanocatalysts [J]. Science, 2007, 317: 100−102.

[32] TAGHINEJAD H, REHN D A, MUCCIANTI C, EFTEKHAR A A, TIAN Meng-kun, FAN Tian-ren, ZHANG Xiang, MENG Yu-ze, CHEN Yan-wen, NGUYEN T V, SHI Su-fei, AJAYAN P M, SCHAIBLEY J, REED E J, ADIBI A. Defect-mediated alloying of monolayer transition-metal dichalcogenides [J]. ACS Nano, 2018, 12: 12795−12804.

[33] GONG Qiu-fang, CHENG Liang, LIU Chang-hai, ZHANG Mei, FENG Qing-liang, YE Hua-lin, ZENG Min, XIE Li-ming, LIU Zhuang, LI Yan-guang. Ultrathin $MoS_{2(1-x)}Se_{2x}$ alloy nanoflakes for electrocatalytic hydrogen evolution reaction [J]. ACS Catalysis, 2015, 5: 2213−2219.

[34] LEE H I, YU H, RHEE C K, SOHN Y. Electrochemical hydrogen evolution and CO_2 reduction over hierarchical MoS_xSe_{2-x} hybrid nanostructures [J]. Applied Surface Science, 2019, 489: 976−982.

[35] LIN Bo, LIN Zhi-ping, CHEN Shou-gang, YU Mei-yan, LI Wen, GAO Qiang, DONG Meng-yao, SHAO Qian, WU Shi-de, DING Tao, GUO Zhan-hu. Surface intercalated spherical $MoS_{2x}Se_{2(1-x)}$ nanocatalysts for highly efficient and durable hydrogen evolution reactions [J]. Dalton Transactions, 2019, 48: 8279−8287.

[36] SHI Hai-yan, ZHANG Hui, LI Mao-jian, WANG Yi, WANG De-zhi. Nanoflower-like 1T/2H mixed-phase $MoSe_2$ as an efficient electrocatalyst for hydrogen evolution [J]. Journal of Alloys and Compounds, 2021, 878: 160381.

[37] XU Ying-shuang, FO Yu-meng, LV Hong-hao, CUI Xue-jing, LIU Guang-bo, ZHOU Xin, JIANG Lu-hua. Anderson-type polyoxometalate-assisted synthesis of defect-rich doped 1T/2H-$MoSe_2$ nanosheets for efficient seawater splitting and Mg/seawater batteries [J]. ACS Applied Materials & Interfaces, 2022, 14: 10246−10256.

[38] YANG Jing, LIU Ying, SHI Chang-shuai, ZHU Ji-xin, YANG Xiao-fei, LIU Si-liang, LI Le, XU Zi-wei, ZHANG Chao, LIU Tian-xi. Carbon nanotube with vertical 2D molybdenum sulphoselenide nanosheet arrays for boosting electrocatalytic hydrogen evolution [J]. ACS Applied Energy Materials, 2018, 1: 7035−7045.

[39] JIAN Chuan-yong, HONG Wen-ting, CAI Qian, LIU Wei. The local electronic structure modulation of the molybdenum selenide–nitride heterojunction for efficient hydrogen evolution reaction [J]. Journal of Materials Chemistry A, 2021, 9: 26113−26118.

[40] ZHAO Xu, ZHAO Yun-dong, HUANG Bin, CAI Wei, SUI Jie-he, YANG Zhi-jian, WANG Hong-en. $MoSe_2$ nanoplatelets with enriched active edge sites for superior sodium-ion storage and enhanced alkaline hydrogen evolution activity [J]. Chemical Engineering Journal, 2020, 382: 123047.

[41] XIE Jun-feng, ZHANG Hao, LI Shuang, WANG Ruo-xing, SUN Xu, ZHOU Min, ZHOU Jing-fang, LOU Xiong-wen, XIE Yi. Defect-rich MoS_2 ultrathin nanosheets with additional active edge sites for enhanced electrocatalytic hydrogen evolution [J]. Advanced Materials, 2013, 25: 5807−5813.

[42] DENG Yun-qie, LIU Zhen, WANG Ai-zhu, SUN De-hui, CHEN Yu-ke, YANG Lin-jing, PANG Jin-bo, LI Hai, LI Hai-dong, LIU Hong, ZHOU Wei-jia. Oxygen-incorporated MoX (X: S, Se or P) nanosheets via universal and controlled electrochemical anodic activation for enhanced hydrogen evolution activity [J]. Nano Energy, 2019, 62: 338−347.

[43] ZHANG Xiao-hong, LI Nan, WU Jiao-jiao, ZHENG Yan-zhen, TAO Xia. Defect-rich O-incorporated 1T-MoS_2 nanosheets for remarkably enhanced visible-light photocatalytic H_2 evolution over CdS: The impact of enriched defects [J]. Applied Catalysis B: Environmental, 2018, 229: 227−236.

[44] QU Yin-dong, MEDINA H, WANG Sheng-wen, WANG Yi-chung, CHEN Chia-wei, SU Teng-yu, MANIKANDAN A, WANG Kuang-ye, SHIH Yu-chuan, CHANG Je-wei, KUO Hao-chung, LEE C Y, LU S, SHEN Guo-zhen, WANG Z M, CHUEH Y L. Wafer scale phase-engineered 1T- and 2H-$MoSe_2$/Mo core–shell 3D-hierarchical nanostructures toward efficient electrocatalytic hydrogen evolution reaction [J]. Advanced Materials, 2016, 28: 9831−9838.

[45] XIA Qing, ZHAO Lan-ling, LI De-yuan, WANG Jun, LIU Li-li, HOU Chuan-xin, LIU Xiao-meng, XU Hao-ran, DANG Feng, ZHANG Jin-tao. Phase modulation of 1T/2H $MoSe_2$ nanoflowers for highly efficient bifunctional electrocatalysis in rechargeable Li−O_2 batteries [J]. Journal of Materials Chemistry A, 2021, 9: 19922−19931.

[46] MAJUMDAR A, DUTTA P, SIKDAR A, LEE H, GHOSH D, JHA S N, TRIPATHI S, OH Y, MAITI U N. Impact of atomic rearrangement and single atom stabilization on $MoSe_2$@$NiCo_2Se_4$ Heterostructure catalyst for efficient overall water splitting [J]. Small, 2022, 18: 2200622.

[47] KIRAN V, MUKHERJEE D, JENJETI R N, SAMPATH S. Active guests in the MoS_2/$MoSe_2$ host lattice: Efficient hydrogen evolution using few-layer alloys of $MoS_{2(1-x)}Se_{2x}$ [J]. Nanoscale, 2014, 6: 12856−12863.

[48] WANG Yi, XIAO Xin-yan, CHEN Jia-yi, LU Ming-li, ZENG Xing-ye. 1T phase boosted $MoSe_2$/pg-C_3N_4 with Z-scheme heterojunction for enhanced photocatalytic degradation of contaminants [J]. Applied Surface Science, 2020, 510: 145341.

[49] GOWRISANKAR A, SHERRYN A L, SELVARAJU T. In situ integrated 2D reduced graphene oxide nanosheets with MoSSe for hydrogen evolution reaction and supercapacitor application [J]. Applied Surface Science Advances, 2021, 3: 100054.

[50] WU Peng-yuan, SUN Gang-yong, CHEN Yuan-zhi, XU Wan-jie, ZHENG Hong-fei, XU Jin, WANG Lai-sen, PENG Dong-Liang. $MoSe_2$-Ni_3Se_4 hybrid nanoelectrocatalysts and their enhanced electrocatalytic activity for hydrogen evolution reaction [J]. Nanoscale Research Letters, 2020, 15: 1−10.

[51] SHARMA M D, MAHALA C, BASU M. 2D Thin sheet heterostructures of MoS_2 on $MoSe_2$ as efficient electrocatalyst for hydrogen evolution reaction in wide pH range [J]. Inorganic Chemistry, 2020, 59: 4377−4388.

[52] MAO Bao-guang, SUN Ping-ping, JIANG Yan, MENG Tao, GUO Dong-lei, QIN Jin-wen, CAO Min-hua. Identifying the transfer kinetics of adsorbed hydroxyl as a descriptor of alkaline hydrogen evolution reaction [J]. Angewandte Chemie International Edition, 2020, 59: 15232−15237.

[53] LI Song-zhan, ZANG Wen-jie, LIU Xi-meng, PENNYCOOK S J, KOU Zong-kui, YANG Chun-hai, GUAN Cao, WANG J. Heterojunction engineering of

$MoSe_2/MoS_2$ with electronic modulation towards synergetic hydrogen evolution reaction and supercapacitance performance [J]. Chemical Engineering Journal, 2019, 359: 1419−1426.

[54] REN Xian-pei, WEI Qing-bo, REN Pin-yun, WANG Yong-hua, CHEN Rong. Synthesis of flower-like $MoSe_2$@ MoS_2 nanocomposites as the high efficient water splitting electrocatalyst [J]. Materials Letters, 2018, 231: 213−216.

[55] ZHAO Long, WEN Ming, TIAN Ya-kun, WU Qing-sheng, FU Yong-qing. A novel structure of quasi-monolayered NiCo-bimetal-phosphide for superior electrochemical performance [J]. Journal of Energy Chemistry, 2022, 74: 203−211.

[56] WANG Zi-fang, TIAN Ya-kun, WEN Ming, WU Qing-sheng, ZHU Quan-jing, FU Yong-qing. Integrating $CoNiSe_2$ nanorod-arrays onto N-doped sea-sponge-C spheres for highly efficient electrocatalysis of hydrogen evolution reaction [J]. Chemical Engineering Journal, 2022, 446: 137335.

[57] FANG Hao, YANG Jin-hu, WEN Ming, WU Qing-sheng. Nanoalloy materials for chemical catalysis [J]. Advanced Materials, 2018, 30: 1705698.

高效析氢用花状 MoS_xSe_{2-x} 纳米复合材料的简便合成

史海燕[1]，汪 异[2]，王德志[1]

1. 中南大学 材料科学与工程学院，长沙 410083；
2. 湖南科技大学 材料科学与工程学院，湘潭 411201

摘 要：为了解决 $MoSe_2$ 导电性差和活性位点有限的问题，通过简便水热工艺合成具有缺陷的三元 MoS_xSe_{2-x} 纳米片。结果表明，硫元素的引入，不仅提高了其电子转移能力，而且提供了更多的电催化活性位点。因此，优化后 S/Se 摩尔比为 1:1 的 MoS_xSe_{2-x}(MoSSe)具有优异的电催化析氢(HER)性能，其 Tafel 斜率仅为 47 mV/dec，在 −10 mA/cm^2 下具有较低的过电位(−165 mV)，并且具有良好的耐久性。这项工作为更好地理解多因素调控在设计和合成 $MoSe_2$ 基催化剂以提高其电化学活性方面提供了一条额外的途径。

关键词：三元 MoS_xSe_{2-x} 合金；缺陷；协同效应；电催化剂；析氢

(Edited by Wei-ping CHEN)